NANOMATERIALS

Atomically precise, custom-design origami graphene nanostructures

Hui Chen[1]*, Xian-Li Zhang[1]*, Yu-Yang Zhang[1,2]*, Dongfei Wang[1], De-Liang Bao[1,2], Yande Que[1], Wende Xiao[1], Shixuan Du[1]†, Min Ouyang[3], Sokrates T. Pantelides[1,2], Hong-Jun Gao[1]†

The construction of atomically precise carbon nanostructures holds promise for developing materials for scientific study and nanotechnology applications. Here, we show that graphene origami is an efficient way to convert graphene into atomically precise, complex nanostructures. By scanning tunneling microscope manipulation at low temperature, we repeatedly fold and unfold graphene nanoislands (GNIs) along an arbitrarily chosen direction. A bilayer graphene stack featuring a tunable twist angle and a tubular edge connection between the layers is formed. Folding single-crystal GNIs creates tubular edges with specified chirality and one-dimensional electronic features similar to those of carbon nanotubes, whereas folding bicrystal GNIs creates well-defined intramolecular junctions. Both origami structural models and electronic band structures are computed to complement analysis of the experimental results. The present atomically precise graphene origami provides a platform for constructing carbon nanostructures with engineered quantum properties and, ultimately, quantum machines.

The discovery of fullerenes, nanotubes, and, more recently, the isolation of monolayer graphene sparked a revolution in the fabrication of a variety of sp^2-bonded carbon allotropes (*1*, *2*). Graphene itself, along with variants that include five- and/or seven-membered rings, can be viewed as building blocks of sp^2-bonded allotropes (*3*), three-dimensional (3D) graphene-based nanostructures (GNSs), and devices that have been either fabricated or predicted theoretically for potential applications (*4*–*7*), even machines (*8*). Experimental realization of GNSs has been pursued by a variety of chemical, electrochemical, mechanical, radiation-assisted, and other approaches (*2*). These approaches, however, lack the ability to produce pure, structurally uniform GNSs, with bottom-up chemical synthesis being viewed by some as the most promising route toward that goal (*9*). Meeting this challenge for GNSs with features < 10 nm that can be used for quantum functionalities is even more demanding, as atomic-level precision is needed.

Origami, the ancient art of paper folding, has been widely used in diverse areas, from architecture to battery design and DNA nanofabrication (*10*). It has also inspired the fabrication or simulation of macroscale origami graphene structures and devices (*11*–*20*), even machines (*21*). Nanoscale graphene origami, however, in which quantum phenomena are expected to be manifest, has been mainly the realm of theoretical investigations, predicting GNSs with unusual physical properties such as an ability to carry spin-polarized currents for spintronic applications (*22*), fold-induced gauge fields (*23*), large permanent electric dipoles (*24*), strong magnetophotoelectric effect (*25*), and topologically protected fold states (*26*). The electronic properties of folded GNSs have been predicted to depend sensitively on detailed atomic configurations (*24*, *27*). In addition, graphene sheets containing particular defects (*28*) can, in principle, be used to create origami GNSs with distinctive functionalization.

The experimental demonstration of atomically precise, nanoscale graphene origami, however, has received limited attention. "Graphite origami" was first envisioned in 1995 by Ebbesen and Hiura (*29*), who observed accidental tearing and folding of graphite surface layers by an atomic force microscope (AFM) tip. In 1998, Roy *et al.* (*30*, *31*) showed that a scanning tunneling microscope (STM) tip can be used to induce the folding of "graphitic sheets" at step edges of graphite but without control of the folding direction. Similar results were reported in 2006 by Li *et al.* (*32*) using an AFM tip. Tearing and deformations were observed. In 2008, Schniepp *et al.* (*33*) achieved folding and unfolding of monolayer graphene but concluded that the folds occur at preexisting kink or fault lines. More recently, Akius and Ruitenbeek reported folding and unfolding of graphene in a V cut made on the top sheet of graphite, but the folding angle was constrained by the "pinning" effect of the graphene edge, and the operation was typically accompanied by tears or damage (*34*). Atomically precise and controllable graphene origami for the creation of custom-design GNSs with quantum features remains an open challenge.

In this paper, we report the atomically precise folding and unfolding of graphene nanoislands (GNIs) on a highly ordered pyrolytic graphite substrate without any tears or damage, including 2D stacked, bilayer graphene with a precisely tunable twisting angle and 1D folded tubular edge, which is associated with intramolecular junctions (IMJs). More specifically, using the tip of an STM, we repeatedly folded GNIs to achieve origami GNSs and unfolded them into their original topography. By controlling folding directions, various stacked, bilayer GNSs possessing an arbitrary twisting angle up to 60° with an accuracy of 0.1° can be fabricated, with the distinctive feature that the bilayer is connected by a tubular edge. The chirality and corresponding electronic properties of as-formed 1D tubular nanostructures on the edges, which resemble carbon nanotubes (CNTs), are precisely controlled. Furthermore, by folding bicrystal GNIs with atomically well-defined domain boundaries, analogs of CNT IMJs have been created, and their electronic properties have been probed by scanning tunneling spectroscopy and compared with density functional theory calculations. Model GNSs were optimized by using classical force fields and used to complement the analysis of experimental images. The present work provides a route for the fabrication of GNSs with engineered properties and the construction of graphene-based quantum machines. Furthermore, the results reported in this paper set the stage for the discovery of new and unusual phenomena, as the folded GNIs are composite structures comprising a CNT-like fold and a twisted bilayer graphene. For example, it may be worth exploring the superconductivity of the twisted bilayer graphene part with a magic twist angle attached to either a semiconducting or metallic tube or an IMJ.

Figure 1, A and B, shows a schematic graphic and experimental demonstration of STM origami by sequentially folding and unfolding a single GNI along a predefined direction, respectively. Briefly, to fold a GNI, an STM tip is brought close to its edge by reducing the tunneling resistance in the STM junction, followed by moving across the GNI along a predetermined direction (arrows; Fig. 1, A and B). During its motion, the tip lifts the GNI by the edge, drags the GNI along the tip's own track, stops, and places the moving portion of the GNI at the desired location. This process results in a folded GNS, in which part of the GNI is vertically stacked on the remaining part to form a 2D bilayer graphene stack that is connected by a 1D tubular edge (Fig. 1C). A reversed process can be performed to unfold the new GNS with full recovery of the original GNI (Fig. 1B). Such folding and unfolding processes can be repeated multiple times with the same GNI along arbitrary directions without causing damage or structural defects. It is, therefore, possible to achieve various desirable GNSs without changing their local environment to facilitate systematic structure-property studies. A few distinctive features of

[1]Institute of Physics and University of Chinese Academy of Sciences, Chinese Academy of Sciences, Beijing 100190, China. [2]Departments of Physics and Astronomy and Electrical Engineering and Computer Science, Vanderbilt University, Nashville, TN 37235, USA. [3]Department of Physics, University of Maryland, College Park, MD 20742, USA.
*These authors contributed equally to this work.
†Corresponding author. Email: hjgao@iphy.ac.cn (H.-J.G.); sxdu@iphy.ac.cn (S.D.)

our STM nano-origami stand out compared with those of structures described in all existing relevant literature (*29*–*34*) and open opportunities for further study that cannot be achieved otherwise: (i) The folding operation is spatially localized [i.e., the operation on one GNI has no effect on its neighbors (fig. S1)]. (ii) The folding direction is arbitrary and atomically precise. (iii) There is no size limitation on the GNIs, which makes it feasible to create folded GNSs at different length scales (fig. S2). (iv) no damage or structural defect has been induced during this repeatable process.

The STM-origami GNSs are of high quality and are atomically well defined. Figure 1C shows atomic arrangements of one typical folded GNS, highlighting two different structural features: a 2D bilayer flatland and a 1D tubular structure on the edge. A line profile across the folded GNS is shown in Fig. 1D. The bilayer nature of the GNS is confirmed by the height between the top layer and the substrate, namely ~0.71 nm, which is comparable to the distance between two graphene layers (~0.70 nm) (*35*). The curved profile of the edge, which is higher than the flat top layer, corroborates its identification as a tubular edge.

We have repeated the folding and unfolding of a GNI along several directions sequentially. The arbitrary folding capability demonstrated in Fig. 1 immediately opens an opportunity to achieve graphene stacking with a tunable twist (Fig. 2A). The twisting angle θ between the top layer and the bottom layer can be determined by the folding direction (the moving direction of the STM tip for the origami operation) (fig. S3). Figure 2B (bottom) shows three exemplary GNSs with distinct folding orientations from the same GNI (top middle). In addition to bilayer stacking, by sequentially folding multiple times, multilayer stacked GNSs can also be obtained (fig. S4). We have found that even after multiple folding and unfolding steps, the overall morphology of GNI remains the same without the appearance of defects, as determined by comparing high-resolution STM images recorded before and after operations (Fig. 2B). These data suggest that STM origami is a safe and gentle operation that is essential for the construction of high-quality stacked structures.

Direct evidence of stacking with different twist angles is the formation of a tunable moiré superstructure on a folded GNS. Figure 2A (bottom) presents typical high-resolution STM images and corresponding models of two different GNSs formed by folding the same GNI along different directions. The folding angles (fig. S3) used for creating these two GNSs are 0.8° and 27.2° and lead to the resultant θ of 1.6° and 54.4°, respectively. This estimation of θ from folding directions shows excellent agreement with the observed moiré superstructures, in which θ can also be directly determined by measuring the periodicity d of the superstructure [$\theta = 2\arcsin(a/2d)$, where a is the graphene lattice constant]. This cross-referencing of the value of θ provides a check for the STM-origami operations and confirms the tunability of twisted stacked GNSs by simply varying the folding direction. Figure 2A (top right), which summarizes the different experimental values of θ that have been achieved in the present work, demonstrates the range and precise control of arbitrary twisting in bilayer graphene made possible by the STM origami.

In addition to the stacked bilayer nanostructures, folding a GNI also generically forms a tubular edge whose chirality depends solely on the folding direction (Fig. 1C). The origami process is essentially the same as the roll-up model of a perfect single-walled CNT from a monolayer graphene except that the as-formed tube is not seamlessly closed in the present work (*36*). We have, therefore, employed the conventional chiral indices notation (n, m) of a CNT to define the constructed tubular edges, where n and m are integers (fig. S5). Figure 3, A and B, shows atomic configurations of two tubular edges constructed from the same GNI but using two different folding directions. In Fig. 3A, the angle between the folding axis and hexagonal lattice is ~3 ± 1°, whereas that in Fig. 3B is 19 ± 1°. Correspondingly, these two single-walled tubes are (10, 8) and (12, 3), respectively (a more detailed analysis is shown in fig. S5). The simulated STM image based on the chiral index assignment is also provided and placed underneath its corresponding STM images for comparison. Our simulations of STM images do not consider the tip-convolution effect that often leads to underestimation of tube diameters (*37*). However, the good agreement between simulated and experimental STM images further confirms our index assignment.

We have also measured dI/dV spectra (I, current; V, voltage) along as-formed tubular edges and presented the data in Fig. 3C. In contrast with the data acquired from the flat bilayer graphene region, a clear manifestation of van Hove singularity (VHS) peaks is observed on both tubular edges, suggesting that although these tubular edges are not seamlessly closed, they still have 1D electronic characteristics. Our experimental observation of the 1D VHS characteristic from the folded tubes is also corroborated by the density functional theory calculations of electronic structures of both folded tubes and conventional single-wall CNTs (fig. S7) (*38*). The consistency of the dI/dV spectra acquired along the same tube suggests the delocalized nature of electronic states intrinsic in a 1D structure as well as the

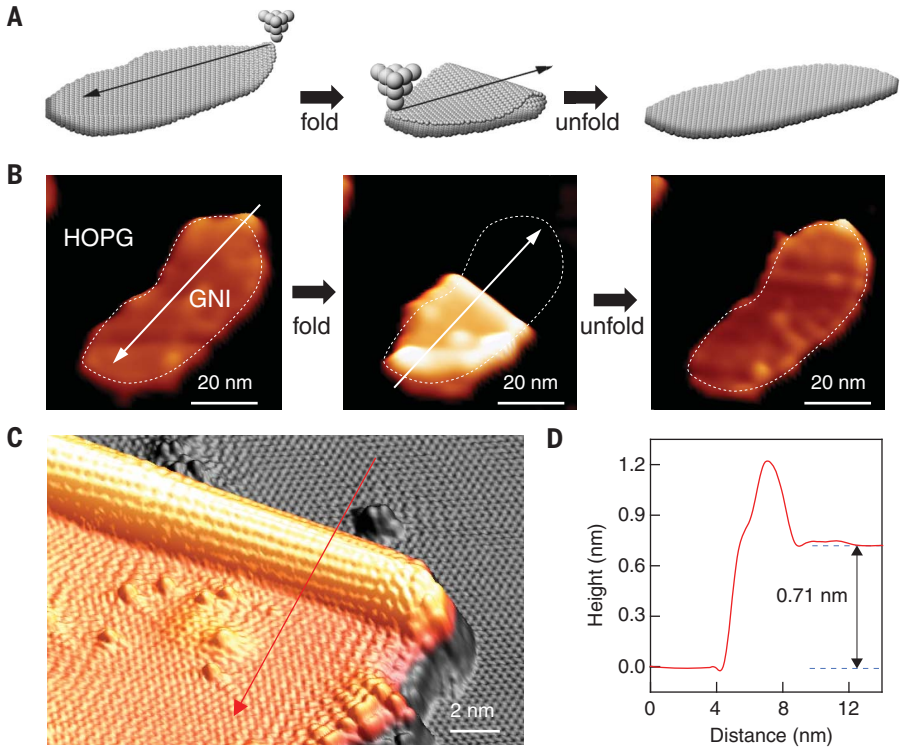

Fig. 1. Construction of atomically well-defined folded GNSs by STM origami. (**A**) Schematic graphic of folding and unfolding a GNI along an arbitrary direction (black arrows). (**B**) Experimental realization of (A). The series of STM images shows a sequence of the folding and unfolding of a GNI along the direction indicated by the white arrows. HOPG, highly ordered pyrolytic graphite. (**C**) 3D STM topography of a typical folded GNS. (**D**) Line profile along the red arrow in (C) showing the formation of both the 1D tubular edge and the 2D stacked graphene flatland with height comparable to the distance between two graphene layers (0.70 nm). Settings for (B): tunneling current I_t = 10 pA; bias voltage V_s = −3 V. Settings for (C): I_t = 100 pA; V_s = 1 V. The GNIs were manipulated by using lateral tip-induced manipulation with a typical current of ~100 pA and a voltage of ~3 mV. All results were acquired at temperature T = 4.2 K.

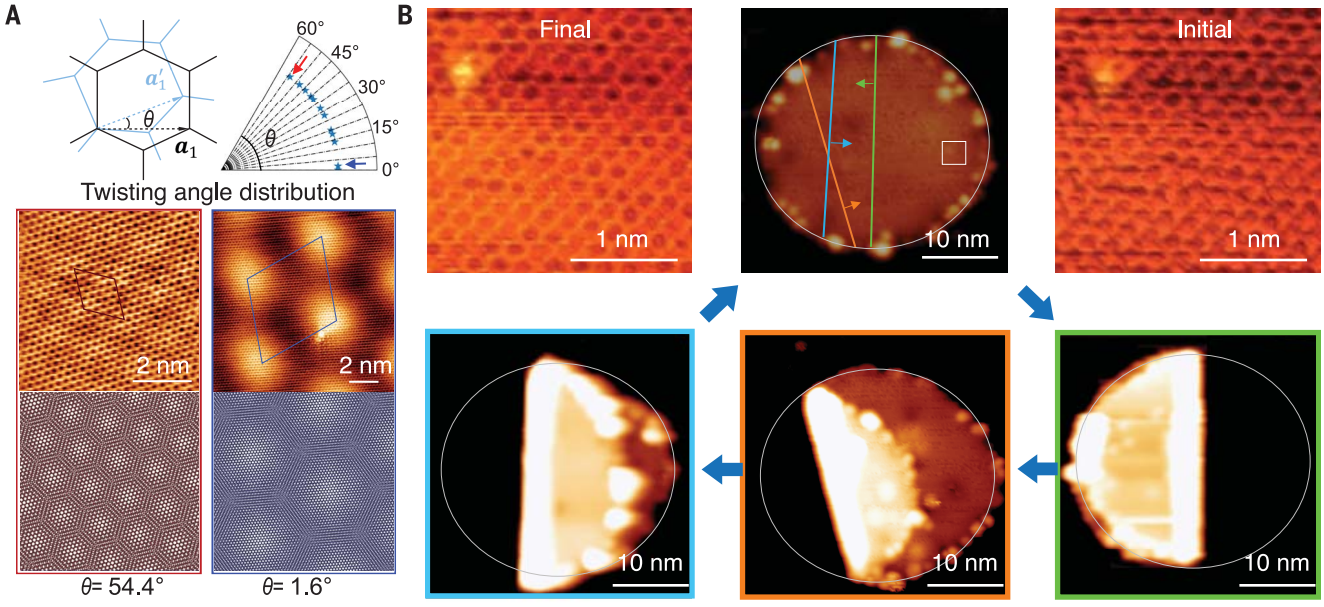

Fig. 2. Precisely controlled folding of a GNI along preselected directions. (**A**) (Top left) Schematic graphic of a 2D bilayer GNS with twisting angle θ produced by folding a GNI. The angle θ can be defined by the folding direction depicted in Fig. 1, A and B (also fig. S3). Light-blue (lattice vector a_1') and black (lattice vector a_1) hexagonal lattices represent the top and bottom layers, respectively. (Top right) Summary of all experimental θ values achieved in the current work showing the tunable range and precise control of θ. (Bottom) STM images and corresponding models showing moiré patterns of two exemplary folded GNSs with different θ: 54.4° and 1.6°, respectively. These two θ values correspond to the red and blue arrow highlights (top right), respectively. Periodic cells are marked by red and blue rhombuses (left and right panels, respectively). (**B**) Series of STM images showing repeatable folding and unfolding of a single GNI along different directions by STM origami. Three examples of folded GNSs from the same GNI (top middle) but different folding directions are shown in the bottom panels. The color frame of each bottom image corresponds to its folding axis, with the same color code marked in the original GNI (top-middle panel). The atomically resolved images in the top-right and top-left panels were acquired from the white square area in the top-middle image before and after multiple origami operations, respectively, showing no occurrence of structural damage. Settings for (A): I_t = 100 pA; V_s = −0.1 V. Settings for (B): I_t = 100 pA; V_s = −0.1 V (top right and top left); I_t = 10 pA; V_s = −3.0 V (others).

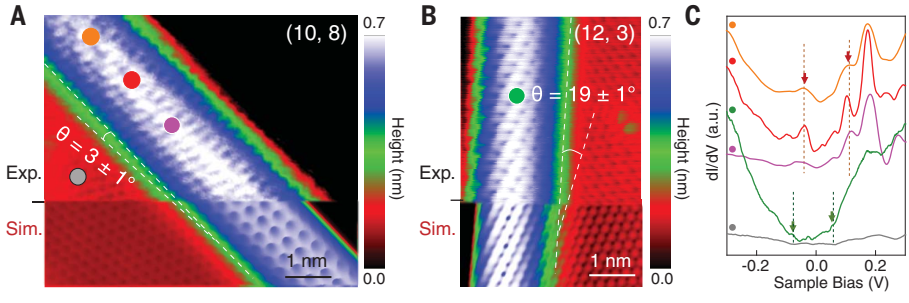

Fig. 3. Tunable 1D tubular carbon structures with different chirality and electronic properties. (**A** and **B**) Atomically resolved STM images showing structural configurations of two chiral tubular structures acquired by folding the same GNI along different directions. The corresponding chiral angle is determined to be 3° and 19° for (A) and (B), respectively. Simulated (Sim.) STM images based on the experimentally determined structural index (fig. S5) are also provided underneath their corresponding experimental (Exp.) images. (**C**) The *dI/dV* spectra acquired at different locations as labeled in (A) and (B) showing the appearance of VHSs and the distinct electronic properties of two different tubular edges. The color codes of the spectra are kept the same as those of location markers in (A) and (B). The red and green dotted lines are guides to show the onset of the first VHS peaks (highlighted by arrows; details are shown in fig. S6) of the two folded tubular structures, respectively. For comparison, the data acquired from the flat region (gray) are also presented. Settings: I_t = 100 pA; V_s = −0.2 V; T = 4.2 K. a.u., arbitrary units.

defect-free quality of the tubes created by the STM origami. Although the two tubular edges presented in Fig. 3, A and B, are created from the same GNI, they show different electronic properties. For example, by comparing their spectra, we find that there exists a small energy shift (31 meV) of the VHS gap from the Fermi energy for the tubular edge in Fig. 3A, which can be attributed to interactions between the tubular edge and the substrate because the (10, 8) tube should behave more as a semiconductor, whereas the (12, 3) tube is more metallic (*39*, *40*). These observations highlight the opportunity to investigate effects of the local environment on low-dimensional electronic properties by using the STM origami.

As we have already demonstrated, STM origami is a general technique that is not limited to perfect single-crystal GNIs. This immediately opens an opportunity to create even more-complex 2D and 1D GNSs that might be challenging otherwise. For example, 1D carbon IMJs consisting of two different CNTs joined by 5–7 structural defects (i.e., defects with a periodic alternation of pentagons and heptagons) forming seamless carbon-based metal-semiconductor, metal-metal, and semiconductor-semiconductor building blocks with robust solid-state behavior (*41*) have been proposed to be perfect molecular-scale electronic devices, such as rectifiers, field-effect transistors,

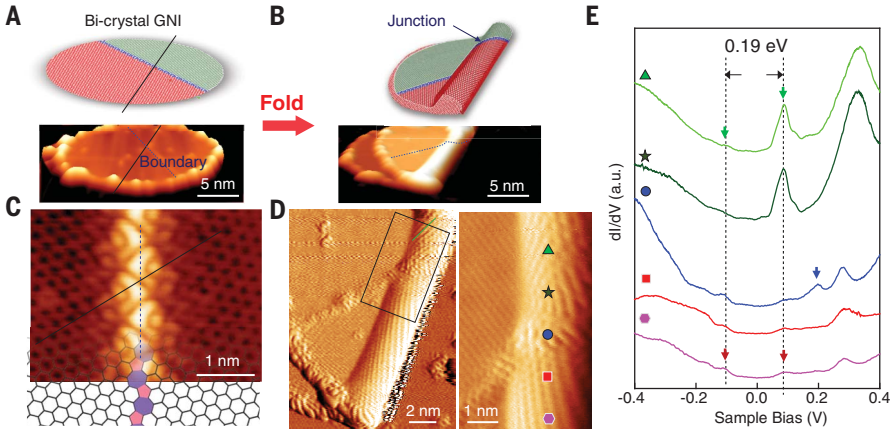

Fig. 4. Creation of 1D carbon IMJs. (**A** and **B**) Schematic diagram (top) and STM image in 3D view (bottom) before (A) and after (B) folding a bicrystal GNI. Red and green shaded regimes represent two different crystalline domains in a bicrystal GNI with a domain boundary (blue dashed line). The black solid line represents the folding axis in the STM origami. (**C**) Atomically resolved STM image revealing the existence of well-defined 5–7 pairs in the boundary of a bicrystal GNI in (A). A 2D structural model of a GNI with a 5–7 pair boundary (alternating orange pentagons and purple heptagons) overlaid on the STM image for structural assignment. (**D**) Atomically resolved STM characterization of the IMJ formed by two folded tubular segments with different chirality (green line segments highlight the chiral vectors of the top tubes). (Left) Large-scale view and (right) zoom-in image of the black rectangular area at left. (**E**) The *dI/dV* spectra recorded at different locations along the IMJ labeled by the color symbols in (D). The two dotted lines are guides to show the evolution of the first VHS peaks along the junction. The blue arrow highlights the appearance of a defect state in the junction interface, which is clearly absent at the location away from the IMJ interface. Settings for (A) and (B): I_t = 10 pA; V_s = −3.0 V. Settings for (C) to (E): I_t = 100 pA; V_s = −0.2 V.

switches, amplifiers, and photoelectrical devices, among others (*42*). These IMJs have been observed experimentally (*43*, *44*), but growth of such IMJs with desirable structural configurations and properties has presented challenges. We have demonstrated that 1D carbon IMJs between dissimilar tubular edges can be created in a highly controlled manner by performing STM origami on a bicrystal GNI (Fig. 4, A and B). Bicrystal GNIs consisting of two different in-plane graphene domains joined by the well-known 5–7 structural defects (figs. S8 and S9) have been successfully achieved recently (*38*). Because our STM origami is a highly spatially localized technique, it can allow selective folding of bicrystal GNIs across 5–7 pair domain boundaries (Fig. 4C) along different directions, leading to an innovative construction of edge IMJs with predefined structures and properties.

Figure 4D shows one example of such an IMJ achieved by STM origami. After folding across a planar 5–7 domain boundary (Fig. 4C), two tubular structures can be resolved with tube indices (9, 4) and (10, 3) for the top and bottom segments, respectively. The difference of chiral vectors between the two segments is ~32°. Accompanying the formation of tubular edges, the 5–7 boundary in the original planar bicrystal GNI is also folded concordantly, forming a well-defined 1D IMJ interface seamlessly joining the two tubular segments. A series of *dI/dV* spectra is also acquired along the IMJ and presented in Fig. 4E. The energy positions of the first two VHSs and corresponding energy gap (0.19 eV) are almost the same for the two connected (9, 4) and (10, 3) tubular edges. This feature can be understood by the fact that both tubes have the same width, and the VHS gap is mainly determined by the tube diameter for semiconducting CNTs (*40*). However, in the junction interface, not only a lattice distortion but also a localized (*dI/dV*) peak at 0.20 eV is clearly observed, which can be attributed to defect states of the 5–7 pairs (*44*). In Fig. 4E, there is a large asymmetry between the two VHS on one side of the junction but not on the other. Such asymmetries are known to exist in CNTs and have been attributed to a variety of effects [(*45*) and references therein]. Differences in lattice deformations are the likely cause.

The emerging IMJ-like structures enabled by STM origami offer a distinctive set of building blocks for demonstrating innovative physical effects and device concepts. Compared with previous work in which IMJs could only be accidentally observed (*42*–*44*), the present method allows for the creation of IMJ-like structures from well-defined 5–7 boundaries, and different combinations of tubular edges can be integrated in a highly selective manner by simply varying the folding direction. Therefore, the present work provides a route to fabricate complex and atomically precise carbon nanostructures with engineered electronic properties that may ultimately lead to the construction of graphene-based quantum machines.

REFERENCES AND NOTES

1. V. Meunier, A. G. Souza Filho, E. B. Barros, M. S. Dresselhaus, *Rev. Mod. Phys.* **88**, 025005 (2016).
2. V. Georgakilas, J. A. Perman, J. Tucek, R. Zboril, *Chem. Rev.* **115**, 4744–4822 (2015).
3. A. K. Geim, K. S. Novoselov, *Nat. Mater.* **6**, 183–191 (2007).
4. L. A. Ponomarenko *et al.*, *Science* **320**, 356–358 (2008).
5. Y. Chen *et al.*, *Nano Lett.* **12**, 1996–2002 (2012).
6. D. Joung *et al.*, *Nano Lett.* **17**, 1987–1994 (2017).
7. S. R. Peurifoy *et al.*, *J. Am. Chem. Soc.* **140**, 9341–9345 (2018).
8. J. Li *et al.*, *Sci. Rep.* **4**, 5846 (2014).
9. Y. Segawa, H. Ito, K. Itami, *Nat. Rev. Mater.* **1**, 15002 (2016).
10. T. Al-Mulla, M. J. Buehler, *Nat. Mater.* **14**, 366–368 (2015).
11. M. J. Allen *et al.*, *Chem. Commun.* **41**, 6285–6287 (2009).
12. B. Wang *et al.*, *Nano Lett.* **17**, 1467–1473 (2017).
13. B. Wang *et al.*, *Adv. Mater.* **30**, e1707449 (2018).
14. J. Mu *et al.*, *Sci. Adv.* **1**, e1500533 (2015).
15. W. Xu *et al.*, *Sci. Adv.* **3**, e1701084 (2017).
16. N. Patra, B. Wang, P. Král, *Nano Lett.* **9**, 3766–3771 (2009).
17. S. Zhu, T. Li, *ACS Nano* **8**, 2864–2872 (2014).
18. W. J. Hyun, O. O. Park, B. D. Chin, *Adv. Mater.* **25**, 4729–4734 (2013).
19. T. Hallam *et al.*, *Nano Lett.* **15**, 857–863 (2015).
20. Y. Wang, V. H. Crespi, *Nano Lett.* **17**, 6708–6714 (2017).
21. M. Z. Miskin *et al.*, *Proc. Natl. Acad. Sci. U.S.A.* **115**, 466–470 (2018).
22. A. T. Costa, M. S. Ferreira, T. Hallam, G. S. Duesberg, A. H. Castro Neto, *Europhys. Lett.* **104**, 47001 (2013).
23. D. Rainis *et al.*, *Phys. Rev. B* **83**, 165403 (2011).
24. J. Feng, L. Qi, J. Y. Huang, J. Li, *Phys. Rev. B* **80**, 165407 (2009).
25. F. Queisser, R. Schützhold, *Phys. Rev. Lett.* **111**, 046601 (2013).
26. E. Prada, P. San-Jose, L. Brey, *Phys. Rev. Lett.* **105**, 106802 (2010).
27. Y. E. Xie, Y. P. Chen, X. L. Wei, J. X. Zhong, *Phys. Rev. B* **86**, 195426 (2012).
28. H. Terrones, R. Lv, M. Terrones, M. S. Dresselhaus, *Rep. Prog. Phys.* **75**, 062501 (2012).
29. T. W. Ebbesen, H. Hiura, *Adv. Mater.* **7**, 582–586 (1995).
30. H. V. Roy, C. Kallinger, B. Marsen, K. Sattler, *J. Appl. Phys.* **83**, 4695–4699 (1998).
31. H. V. Roy, C. Kallinger, K. Sattler, *Surf. Sci.* **407**, 1–6 (1998).
32. L. X. Li *et al.*, *Carbon* **44**, 1544–1547 (2006).
33. H. C. Schniepp *et al.*, *ACS Nano* **2**, 2577–2584 (2008).
34. K. Akius, J. V. Ruitenbeek, arXiv:1812.09501 [cond-mat.mes-hall] (22 December 2018).
35. A. Luican, G. H. Li, E. Y. Andrei, *Solid State Commun.* **149**, 1151–1156 (2009).
36. M. Ouyang, J. L. Huang, C. M. Lieber, *Acc. Chem. Res.* **35**, 1018–1025 (2002).
37. G. I. Márk, L. P. Biró, J. Gyulai, *Phys. Rev. B* **58**, 12645–12648 (1998).
38. Materials and methods are available as supplementary materials.
39. S. M. Bachilo *et al.*, *Science* **298**, 2361–2366 (2002).
40. T. W. Odom, J.-L. Huang, P. Kim, C. M. Lieber, *Nature* **391**, 62–64 (1998).
41. L. Chico, V. H. Crespi, L. X. Benedict, S. G. Louie, M. L. Cohen, *Phys. Rev. Lett.* **76**, 971–974 (1996).
42. D. C. Wei, Y. Q. Liu, *Adv. Mater.* **20**, 2815–2841 (2008).
43. Z. Yao, H. W. C. Postma, L. Balents, C. Dekker, *Nature* **402**, 273–276 (1999).
44. M. Ouyang, J.-L. Huang, C. L. Cheung, C. M. Lieber, *Science* **291**, 97–100 (2001).
45. L. Meng *et al.*, *Phys. Rev. B* **87**, 205405 (2013).

ACKNOWLEDGMENTS

Funding: This work was financially supported by the National Natural Science Foundation of China (nos. 61888102 and 51872284), National Key Research and Development Projects

of China (2016YFA0202300 and 2018YFA0305800), the Strategic Priority Research Program of the Chinese Academy of Sciences (no. XDB30000000), the CAS Pioneer Hundred Talents Program, the Beijing Nova Program (no. Z181100006218023), and the International Partnership Program of the Chinese Academy of Sciences (no. 112111KYSB20160061). M.O. acknowledges support from the Office of Naval Research (N000141712885) and National Science Foundation (DMR1608720). Work at Vanderbilt University (S.T.P., Y.-Y.Z., and D.-L.B.) was supported by the U.S. Department of Energy (grant DE-FG02-09ER46554) and the McMinn Endowment. Computations at Vanderbilt University were carried out at the National Energy Research Scientific Computing Center, a DOE Office of Science User Facility supported by the Office of Science of the U.S. Department of Energy (contract no. DE-AC02-05CH11231). **Author contributions:** H.-J.G. designed the experiments. H.C., D.W., Y.Q., and W.X. prepared the sample and performed the STM experiments. X.-L.Z., Y.-Y.Z., and D.-L.B. performed the calculations and provided theoretical models and explanations under the guidance of S.D. H.C., Y.-Y.Z., S.D., M.O., S.T.P., and H.-J.G. analyzed the experimental data, plotted the figures, and wrote the manuscript. H.-J.G. and S.D. supervised the project. **Competing interests:** The authors declare that they have no competing interests. **Data and materials availability:** The data presented in this paper can be found in the supplementary materials.

SUPPLEMENTARY MATERIALS

science.sciencemag.org/content/365/6457/1036/suppl/DC1
Materials and Methods
Supplementary Text
Figs. S1 to S9
References (*46*–*56*)

23 April 2019; accepted 8 August 2019
10.1126/science.aax7864

Science

Atomically precise, custom-design origami graphene nanostructures

Hui Chen, Xian-Li Zhang, Yu-Yang Zhang, Dongfei Wang, De-Liang Bao, Yande Que, Wende Xiao, Shixuan Du, Min Ouyang, Sokrates T. Pantelides and Hong-Jun Gao

Science **365** (6457), 1036-1040.
DOI: 10.1126/science.aax7864

Precisely folding nanographene

Graphene nanostructures that would result from folding or rolling graphene monolayers or bilayers have been predicted to have a number of interesting electronic properties, but control over such folding processes has been limited. Chen *et al.* used a scanning tunneling microscope tip to fold and unfold graphene nanoislands etched on graphite surfaces at low temperatures (4 kelvin). The fold angle could be precisely controlled to create different twist angles in bilayer graphene and a tubelike edge in folded graphene. They also folded 5 ring–7 ring defects and explored this heterojunction with scanning tunneling spectroscopy.

Science, this issue p. 1036